Design of a New Differential Chaos-Shift-Keying System For Continuous Mobility

Francisco J. Escribano, *Member, IEEE*, Georges Kaddoum, *Member, IEEE*, Alexandre Wagemakers, and Pascal Giard, *Member, IEEE*

***Abstract*—Conventional Differential Chaos-Shift-Keying systems (DCSK) are not the most suitable for supporting continuous-mobility scenarios. Therefore, in this paper an improved Continuous-Mobility Differential Chaos-Shift-Keying system (CM-DCSK) is presented that provides greater agility and improved performance in fast fading channels without accurate channel estimation while still being simple compared to a conventional DCSK system. A new DCSK frame signal is designed to reach this goal. In our new frame design, each reference sample is followed by a data carrier sample. This modification of the system design reduces the hardware complexity of DCSK because it requires a shorter wideband delay line, and significantly improves the performance over fast fading channels while keeping the non-coherent nature of the transmission system. Once the design is explained, the bit error rate performance is computed over a multipath fast fading channel and compared to the conventional DCSK system. Simulation results confirm the advantages of this new non-coherent spread-spectrum design that can support mobility.**

***Index Terms*—Chaos based non-coherent communication system, DCSK system, Fast fading channel, Performance analysis.**

I. Introduction

CHAOTIC signals are one of the hot topics in the field of wireless communications due to their properties [1]–[7]. Notably, their inherent wideband characteristics make them well suited for spread-spectrum schemes [1], [2], [8]. Chaotic sequences have similar advantages to other spread-spectrum ones, including the counteraction of fading effects and jamming resistance. Furthermore, the low probability of interception (LPI) of some chaotic signals allows them to be one of the natural candidates for military scenarios as well as densely populated environments [9], [10]. Additionally, chaos-based sequences have proved to be better candidates than Gold or independent and identically distributed sequences to reduce the peak-to-average power ratio (PAPR) [1], [11].

In the last two decades, many chaos-based communication systems have been proposed [4], [12]–[22]. Chaos-shift-keying (CSK) systems [8] require coherent receivers in order to regenerate an exact replica of the chaotic sequence. However, chaotic synchronization performs poorly in noisy environments [8], and this poses a real challenge for chaotic communication with coherent receivers. Within the class of systems allowing non-coherent reception, differential chaos-shift keying (DCSK) [14], [16], [23] is one of the most studied system. It was shown to be implementable with low complexity [24]. In DCSK, each bit duration is split into two equal slots, where the first slot is allocated to a reference chaotic signal, while the second slot is used to transmit the data spread with the reference signal. The differential nature of this design avoids chaotic synchronization at the receiver side. The performance of DCSK over slow fading has already been studied [25], as well as in cooperative or MIMO schemes [3]–[5], [26], [27].

DCSK is robust to multipath slow fading [28] and demodulation can be carried out without accurate channel state information (CSI) [16], but only if the channel coefficients remain constant during each DCSK bit duration. The major disadvantages of the conventional DCSK design are its poor information security ability due to the repetition of chaos sequences, its poor performance under fast fading, and the need of long wideband delay lines. The latter makes DCSK systems very challenging to implement with current CMOS technologies [29], [30].

There has been a number of proposals to overcome the weaknesses of DCSK. In [31], the authors introduced a time permutation in the DCSK frame which destroys the similarity between the reference and data samples. It makes the bit rate undetectable from spectral analysis while allowing multiple access communications by assigning different permutation functions to each user. Another scheme was proposed by the same authors in [32]: a correlation delay-shift-keying (CDSK) system where the reference and data sequences are transmitted simultaneously in order to increase the data rate and security, but at the cost of a bit-error rate (BER) performance loss. In [33], a multiresolution M-ary DCSK system is proposed, making it possible to manage the tradeoffs of BER and quality of service while keeping the properties of DCSK.

To avoid the use of long delay lines in the implementation of DCSK, a system called code-shifted DCSK (CS-DCSK) [29] has been proposed, where the reference and data sequences are multiplexed using Walsh code sequences instead of resorting to time delay multiplexing. An extended version of this scheme is detailed in [30], where the Walsh codes are replaced by chaotic sequences while the reference signal is transmitted through orthogonal frequencies. These two methods increase the data rate while improving the BER, but require synchronization at

F. J. Escribano is with the University of Alcalá de Henares, Pza. San Diego, s/n, 28801 Alcalá de Henares, Madrid, Spain (e-mail: francisco.escribano@ieee.org).

G. Kaddoum, is with the Dept. of Electr. Eng., École de technologie supérieure, Montréal, Québec, Canada (e-mail: georges.kaddoum@etsmtl.ca)

A. Wagemakers is with Universidad Rey Juan Carlos, Physics Department, C/ Tulipán s/n, 28933 Móstoles, Madrid, Spain, (e-mail: alexandre.wagemakers@urjc.es)

P. Giard, is with the Dept. of Electr. and Comput. Eng., McGill University, Montréal, Québec, Canada (e-mail: pascal.giard@mail.mcgill.ca).

The final publication is available at http://doi.org/10.1109/TCOMM.2016.2538236

the receiver. In [7], a multi-carrier DCSK (MC-DCSK) system is proposed. It can support multi-user transmission [34]. The chaotic reference sequence is transmitted over a predefined subcarrier frequency while multiple modulated data streams are transmitted over the remaining subcarriers. This scheme has improved energy efficiency, offers higher data rates, but has larger bandwidth requirements.

All these schemes are hindered by their high complexity, but they highlight the importance of decoding the transmitted data without the use of a complex channel estimator. However, DCSK systems only work when the channel coefficients remain constant during each bit duration. Continuous mobility implies fast variations of the wireless channel state, and the systems mentioned above fail to recover the data when the channel coefficients vary during the bit duration.

The main motivation of the present paper is to propose a low-complexity, non-coherent, DCSK scheme with shortened wideband delay lines, that may perform well in fast fading channels without the need of accurate CSI. The possibility of using a shortened delay line helps to mitigate the mentioned implementation drawbacks associated to longer ones [29], [30]. To reach this goal, a new DCSK frame is proposed, where each chaotic reference sample is followed by the same reference sample multiplied by the sign associated to the binary data. In this case, the DCSK frame corresponding to a given bit is composed of a sequence of paired samples.

At the receiver side, the signal is correlated with a one time chip T_c delayed version of itself and then sampled with period $2T_c$. After sampling, the sequence is integrated over the whole bit duration. Finally, the decoded bits are recovered by comparing the correlator output to a zero threshold. In this scenario, the adaptation to the wireless channel is naturally performed.

We derive the analytical bit error probability expression over a fast fading channel for the most general case, and we show the accuracy of our analysis by comparing it against numerical simulations. This analysis is valid for any kind of spreading sequence, not just chaos-based ones, but we particularize it for the DCSK case according to the scope of this work. We provide approximate bounds and semi-analytical results which are valuable for practical implementations. We can conclude that this design may be well suited for vehicle-to-vehicle communications or any other mobility scenarios where channel coefficients vary faster than the bit duration.

The remainder of this paper is organized as follows. In Section II, the conventional DCSK is presented along with the architecture of the proposed CM-DCSK system. The performance analysis is developed in Section III. Simulation results and discussions are presented in Section IV. Finally, concluding remarks are presented in Section V.

II. A Spread-spectrum communication system for continuous mobility

In this section, a non-coherent spread-spectrum communication system adapted for a continuous-mobility scenario is presented. A non-coherent spread-spectrum system based on a reference signal can work well under slow fading, but a fast fading context may lead to severe degradation and complete data loss.

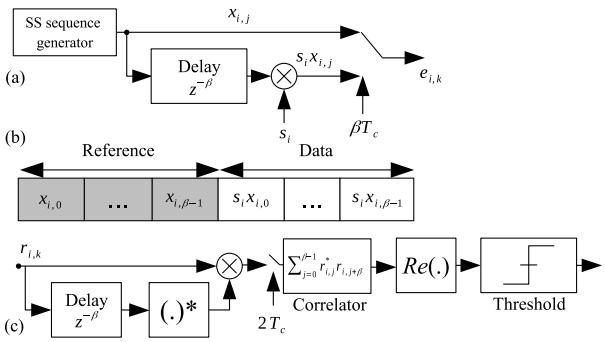

Fig. 1. Block diagram of the general structure of a DSS system. (a) is the DSS transmitter, (b) represents the DSS frame, and (c) is the DSS receiver.

A. Differential spread-spectrum communication systems

The developments proposed in this section are general i.e. not bound to a specific kind of spreading sequence. Thus a general naming convention is used up until Section IV where simulation results are presented and where the focus is on the specific case of DCSK.

The discrete-time baseband equivalent model for a binary conventional differential spread-spectrum (DSS) communication system is shown in Fig. 1. Such a system receives the name of DCSK when chaos-based spreading sequences are used. Fig. 1 shows that, in the modulator, each data value $s_i = \{-1, +1\}$ (a polar binary sequence) is transmitted by using a reference sequence, followed by the reference sequence times the data.

Let 2β be the spreading factor of the DSS system, defined as the number of chips sent for each data bit, where β is an integer, and $T_b = 2\beta T_c$ is the bit duration. During the i^{th} bit interval, and the k^{th} chip period, the output of the transmitter $e_{i,k}$, $k = 0, \cdots, 2\beta - 1$, is defined as

$$e_{i,j} = x_{i,j} \qquad \text{for } 0 \leq j \leq \beta - 1, \tag{1}$$

$$e_{i,j+\beta} = s_i x_{i,j} \qquad \text{for } 0 \leq j \leq \beta - 1, \tag{2}$$

where $x_{i,j}$ is the j^{th} sample of the spreading sequence for the i^{th} bit. The spreading-sequence power is normalized so that $\mathrm{E}\left[|x_{i,j}|^2\right] = 1$, and, therefore, $\mathrm{E}\left[|e_{i,k}|^2\right] = 1$.

The DSS receiver in Fig. 1c illustrates how the first half of the received chip samples, $r_{i,j+\beta}$, $j = 0, \cdots, \beta - 1$, is correlated with the conjugated second-half part of the sequence, $r^*_{i,j}$, $j = 0, \cdots, \beta - 1$; the result is sampled with period $2T_c$ and accumulated over half the bit duration (β samples). Lastly, the data is estimated through a thresholding operation.

B. CM-DSS system design

The continuous-mobility differential spread-spectrum (CM-DSS) design proposed here aims to support a continuous-mobility scenario, and this implies a fast change in the channel

coefficients with respect to the bit rate. The discrete-time baseband equivalent model is shown in Fig. 2. The transmission of a bit requires again two sequences of spread-spectrum samples, so that we can still differentially demodulate the data. However, unlike the conventional DSS setup that separately spans the reference samples and the data-carrying samples in different intervals of durationg $T_b/2$, the CM-DSS transmitter uses a short delay circuit of one chip period T_c *for each type of sample*. Such a circuit is easy to implement in CMOS technology.

This new strategy generates a novel spread-spectrum frame, that can significantly increase the resistance of the system to possible fast variations of the channel coefficients during the overall transmission bit period. Again, 2β defines the spreading factor such that $T_b = 2\beta T_c$. The length of the reference sequence is the same as in the DSS setup, the only change lies in the definition of the frame. This CM-DSS system benefits from the non-coherent advantages of a differential spread-spectrum system, along with improved resistance to fast fading channels, as will be shown in the sequel. The key point here is the low implementation complexity.

During the i^{th} bit interval, and the k^{th} chip time, the output of the transmitter $e_{i,k}$, $k = 0, \cdots, 2\beta - 1$, can be described as

$$e_{i,2j} = x_{i,j} \quad \text{for } 0 \leq j \leq \beta - 1, \tag{3}$$

$$e_{i,2j+1} = s_i x_{i,j} \quad \text{for } 0 \leq j \leq \beta - 1, \tag{4}$$

where $x_{i,j}$ is the spread-spectrum sequence sample.

As shown in Fig. 2c, the block diagram of the CM-DSS receiver, the conjugated received sequence sample $r^*_{i,2j}$ is correlated with a delayed version of itself $r_{i,2j+1}$. The result is then sampled with sampling period $2T_c$ and accumulated over β chip periods. Again, the received bits are estimated through a thresholding operation. With this strategy, even if the channel coefficients change during time $T_b = 2\beta T_c$, the CM-DSS receiver could still recover the data with some reliability. If the channel response is constant during a number of T_c periods, the reference and data samples may be successfully correlated. The degree of compensation depends on the coherence time of the channel relative to the bit and chip periods. This point is detailed and mathematically analyzed in Section III, the performance analysis section of this paper.

C. Channel model

We choose a commonly used channel model in spread-spectrum wireless communication systems, valid to represent both fast or slow flat fading. A two-ray Rayleigh channel model is used in similar chaos-based spread-spectrum systems [28], [16]. A general model could be as shown in Fig.3, where we represent schematically a multipath fading channel with L ($L \geq 2$) independent paths. In the analytic part, we will begin by considering the two-ray model for convenience. After this, we will show how to take into account the general case with $L \geq 2$ multipath components.

In the model of Fig. 3, λ_l is the complex channel coefficient of the l^{th} path. We will use the notation $\lambda_{l,i,k}$ for the channel coefficient from the l^{th} path affecting the k^{th} chip of the i^{th} bit. We consider the first path to be synchronously detected

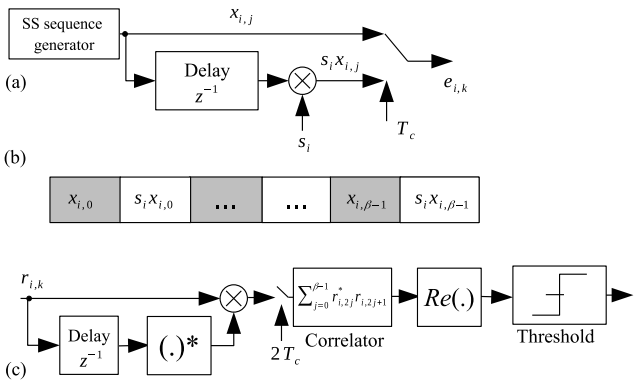

Fig. 2. Block diagram of the general structure of the CM-DSS system. (a) is the CM-DSS transmitter, (b) represents the CM-DSS frame, and (c) is the CM-DSS receiver

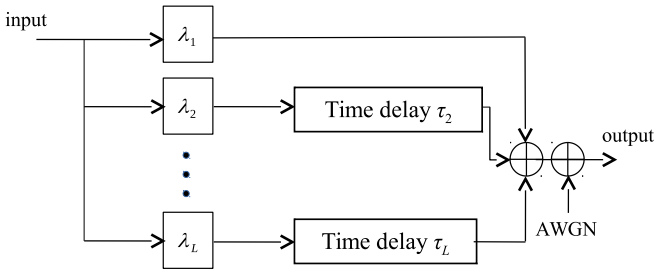

Fig. 3. Multipath fading channel model.

(main path, no delay in the figure), while the rest of paths are received with different time delays τ_l, for $l > 1$. As we work with baseband equivalents of sampled signals, the delay for the l^{th} path in terms of number of chips will be denoted as d_l, which is an integer greater or equal than 0. Note that $d_1 = 0$. We are going to assume that $d_l < \beta$, i.e. the path delay will always be shorter than half the bit duration.

Each channel flat-fading coefficient λ_l corresponds to a general Rician model with expression

$$\lambda_l = g_l \cdot \left[\sqrt{\frac{K}{1+K}} + \sqrt{\frac{1}{1+K}} \cdot (r_I + j r_Q) \right], \tag{5}$$

where K is the ratio of specular to diffuse energy [35], g_l is a real number representing the path gain, and r_I and r_Q are $\mathcal{N}(0, 1/2)$ random variables (RVs). The first term inside the brackets represent the line-of-sight (LOS) component of the channel, whereas the second term represents the dispersive component. When $K = 0$ we are in the pure Rayleigh fading case, whereas $K \to \infty$ represents a channel without fading. Let $a = |\lambda_l| / g_l$ be the normalized envelope of the fading coefficient, we may verify that it constitutes a Rician RV with probability density function (pdf) [35]

$$p(a) = 2a(1+K) e^{-a^2(1+K) - K} I_0 \left(2a\sqrt{K(K+1)} \right), \tag{6}$$

where $I_0(\cdot)$ is the zeroth-order modified Bessel function of the first kind, and $a \geq 0$. Note that $\mathrm{E}\left[a^2\right] = 1$. We assume that the main path may exhibit a LOS component and therefore

$|\lambda_1|/g_1$ follows (6) with $K \geq 0$, while the rest of paths $|\lambda_l|/g_l$, $l > 1$, follow a Rayleigh pdf ($K = 0$). This is a reasonable model, as stated in [35]. We also assume that $\sum_{l=1}^{L} g_l^2 = 1$.

Dropping for the moment the bit index i, the autocorrelation of the fading coefficients is determined by $R_{\lambda_l}[m] = \mathrm{E}\left[\lambda_{l,k} \cdot \lambda_{l,k+m}^*\right]$, and the Doppler power spectral density (psd) is given by its discrete Fourier transform. We follow the known Jakes' model [35], where, for $K = 0$,

$$S_{\lambda_l}(\omega) = \mathcal{F}\{R_{\lambda_l}[m]\} = \frac{g_l^2}{\pi f_{d_l}\sqrt{1-\left(\frac{\omega}{2\pi f_{d_l}}\right)^2}}, \tag{7}$$

where f_{d_l} is the Doppler frequency for the l^{th} path. The autocorrelation of any λ_l is then

$$R_{\lambda_l}[m] = g_l^2\left(\frac{K}{1+K} + \frac{1}{1+K}J_0(2\pi m f_{d_l} T_c)\right), \tag{8}$$

where T_c is the chip period and $J_0(\cdot)$ is the zeroth-order Bessel function of the first kind. We will use a standard definition of the coherence time as [36]

$$T_{ch_l} = \frac{9}{16\pi f_{d_l}}. \tag{9}$$

The parameter used for analysis and simulations will be the coherence time normalized to the chip period, as

$$N_{\lambda_l} = \frac{T_{ch_l}}{T_c}. \tag{10}$$

Taking all this into account, the received signal $r_{i,k}$ for the i^{th} symbol interval and the k^{th} chip time ($k = 0, \cdots, 2\beta - 1$) will be

$$r_{i,k} = \sum_{\substack{l=1 \\ k-d_l \geq 0}}^{L} \lambda_{l,i,k-d_l} \cdot e_{i,k-d_l} + \tag{11}$$
$$+ \sum_{\substack{l=2 \\ k-d_l < 0}}^{L} \lambda_{l,i-1,k-d_l+2\beta} \cdot e_{i-1,k-d_l+2\beta} + n_k$$

where n_k is a sample of the AWGN process for chip time k, and $n_k = n_k^I + j \cdot n_k^Q$, where each noise component is a Gaussian RV with variance σ_n^2. Given that ($\mathrm{E}\left[|e_{i,k}|^2\right] = 1$), noise power calculations will be related to E_b/N_0 following

$$\mathrm{E}\left[|n_k|^2\right] = 2\sigma_n^2 = \frac{2\beta}{E_b/N_0}. \tag{12}$$

Note that, for a given delay d_l and given values of k lower than such a delay, we have an interference term from the previous data symbol sequence. Under slow fading, the value of $\lambda_{l,i,k}$ for a given l^{th} path and a given i^{th} bit period will change slowly throughout the sequence, and will keep a highly correlated value for a given number of chip periods. In a continuous-mobility scenario, we may have a situation where $\lambda_{l,i,k}$ changes in an almost uncorrelated way at each k^{th} chip period for given l and i. This will have an impact on the possibilities of the CM-DSS model, as will be shown in the subsequent analysis.

III. Performance analysis of CM-DSS

In this section, the performance of the CM-DSS and DSS setups is evaluated, and the analytical BER expression for CM-DSS is derived. The focus is on the two-path model. This model captures the majority of cases of practical interest i.e. where the main interference comes from a secondary well defined set of scatterers with significant power, thus constituting a distinguishable—second—path. From three paths and on, their joint effects on the recovered signal converge rapidly to an equivalent model with lots of scatterers building up a single—equivalent—faded path.

The decision variable is the input to the thresholding block of Figs. 1 and 2. Considering the DSS case, we have, for the m^{th} symbol interval:

$$D_m = \frac{1}{\beta} \cdot \Re\left[\sum_{j=0}^{\beta-1} r_{m,j}^* \cdot r_{m,j+\beta}\right], \tag{13}$$

where

$$\begin{gathered} r_{m,k} = \lambda_{1,m,k} e_{m,k} + \\ + \lambda_{2,m-1,k-d_2+2\beta} e_{m-1,k-d_2+2\beta} + n_k, \\ 0 \leq k \leq d_2 - 1, \\ r_{m,k} = \lambda_{1,m,k} e_{m,k} + \lambda_{2,m,k-d_2} e_{m,k-d_2} + n_k, \\ d_2 \leq k \leq 2\beta - 1. \end{gathered} \tag{14}$$

The decision rule consists in choosing $\hat{s}_m = +1$ when $D_m > 0$, and $\hat{s}_m = -1$ when $D_m < 0$. The correlation inside the brackets of expression (13) can be unfolded into

$$\begin{aligned} \sum_{j=0}^{\beta-1} r_{m,j}^* \cdot r_{m,j+\beta} = \sum_{j=0}^{d_2-1} (\lambda_{1,m,j} e_{m,j} + \\ + \lambda_{2,m-1,j-d_2+2\beta} e_{m-1,j-d_2+2\beta} + n_j)^* \cdot \\ \cdot (\lambda_{1,m,j+\beta} e_{m,j+\beta} + \lambda_{2,m,j-d_2+\beta} e_{m,j-d_2+\beta} + n_{j+\beta}) + \\ + \sum_{j=d_2}^{\beta-1} (\lambda_{1,m,j} e_{m,j} + \lambda_{2,m,j-d_2} e_{m,j-d_2} + n_j)^* \cdot \\ \cdot (\lambda_{1,m,j+\beta} e_{m,j+\beta} + \lambda_{2,m,j-d_2+\beta} e_{m,j-d_2+\beta} + n_{j+\beta}), \end{aligned} \tag{15}$$

where we have a number of terms with different impacts on the decision variable, depending on the delay and change rate profile of the $L = 2$ path. Let's examine the main term contributing to the information recovery, the autocorrelation of the first path:

$$\begin{aligned} \sum_{j=0}^{\beta-1} \lambda_{1,m,j}^* \lambda_{1,m,j+\beta} e_{m,j}^* e_{m,j+\beta} = \\ = s_m \cdot \sum_{j=0}^{\beta-1} \lambda_{1,m,j}^* \lambda_{1,m,j+\beta} |x_{m,j}|^2 \end{aligned} \tag{16}$$

where $|x_{m,j}|^2$ stems from a deterministic spreading sequence. Given the phase statistics of the λ random variable as seen in (5), and assuming a scenario where the coherence time is lower than T_c, $\lambda_{1,m,j}^*$ and $\lambda_{1,m,j+\beta}$ will be almost fully uncorrelated

and the expectation of (16) yields

$$\begin{aligned}&\mathrm{E}\left[\Re\left[s_m\sum_{j=0}^{\beta-1}\lambda_{1,m,j}^{*}\lambda_{1,m,j+\beta}|x_{m,j}|^2\right]\right]=\\&=s_m\sum_{j=0}^{\beta-1}|x_{m,j}|^2\Re\left[\mathrm{E}\left[\lambda_{1,m,j}^{*}\lambda_{1,m,j+\beta}\right]\right]=\\&=s_m\sum_{j=0}^{\beta-1}|x_{m,j}|^2\Re\left[\mathrm{E}\left[\lambda_{1,m,j}^{*}\right]\mathrm{E}\left[\lambda_{1,m,j+\beta}\right]\right]=\\&=s_m\cdot g_1^2\cdot\tfrac{K}{1+K}\sum_{j=0}^{\beta-1}|x_{m,j}|^2.\end{aligned}\tag{17}$$

This expression tends to 0 when we are close to the purely Rayleigh scenario, so that $K\to 0$. Therefore, in such situation, the DSS approach cannot recover the data sent. The information may be fully destroyed, unless the LOS component is clearly dominant.

Let us now examine what happens in the CM-DSS case. The decision variable is defined as

$$D_m=\frac{1}{\beta}\cdot\Re\left[\sum_{j=0}^{\beta-1}r_{m,2j}^{*}\cdot r_{m,2j+1}\right].\tag{18}$$

Assuming knowledge of both fading sequences

$$\begin{aligned}\boldsymbol{\lambda}_1&=\left(\lambda_{1,m,0},\cdots,\lambda_{1,m,2\beta-1}\right),\\\boldsymbol{\lambda}_2&=\left(\lambda_{2,m-1,2\beta-d_2},\cdots,\lambda_{2,m-1,2\beta-1},\right.\\&\qquad\left.\lambda_{2,m,0},\cdots,\lambda_{2,m,2\beta-1-d_2}\right),\end{aligned}\tag{19}$$

and in order to calculate conditional probabilities on $\boldsymbol{\lambda}_1$ and $\boldsymbol{\lambda}_2$, we can decompose D_m, for d_2 even, into a number of discrete contributions, containing data recovery and interference terms. The calculations involved are given in Appendix A. As explained there, D_m results in a Gaussian RV with conditional pdf

$$\begin{aligned}&f_{D_m}\left(z\,|s_m,s_{m-1},\boldsymbol{\lambda}_1,\boldsymbol{\lambda}_2\right)=\\&=\frac{1}{\sqrt{2\pi}\sigma_{D_m}(s_m,s_{m-1})}\cdot\mathrm{e}^{-\frac{\left(z-\eta_{D_m}(s_m,s_{m-1})\right)^2}{2\sigma_{D_m}^2(s_m,s_{m-1})}},\end{aligned}\tag{20}$$

where the variance consists in the contribution of terms (35), (37), (38)

$$\sigma_{D_m}^2(s_m,s_{m-1})=\sigma_1^2+\sigma_2^2+\sigma_3^2(s_m,s_{m-1})\tag{21}$$

and the mean in the contribution of terms (36), (39), (40), (41), (42), (43), (44)

$$\begin{aligned}\eta_{D_m}(s_m,s_{m-1})&=\eta_1(s_m)+\eta_2(s_{m-1})+\eta_3(s_m)+\\&+\eta_4(s_m)+\eta_5(s_m)+\eta_6(s_{m-1})+\eta_7(s_m).\end{aligned}\tag{22}$$

The case with delay d_2 odd yields similar results. The derivations are given in Appendix B. The total variance of the Gaussian RV encompasses the contribution of terms (35), (54), (55)

$$\sigma_{D_m}^2(s_m,s_{m-1})=\sigma_1^2+\sigma_2^2(s_{m-1},s_m)+\sigma_3^2(s_m)\tag{23}$$

and the mean, the contribution of terms (36), (45), (46), (47), (48), (49), (50), (51), (52), (53)

$$\begin{aligned}\eta_{D_m}(s_m,s_{m-1})&=\eta_1(s_m)+\eta_2+\eta_3(s_{m-1},s_m)+\\&+\eta_4(s_{m-1})+\eta_5+\eta_6(s_{m-1},s_m)+\eta_7(s_{m-1})+\\&+\eta_8+\eta_9+\eta_{10}(s_m).\end{aligned}\tag{24}$$

Note that the mean and variance have some specificities depending on whether the delay of the second path d_2 is odd or even. Very remarkably, when it is odd, we have some bias terms in η_{D_m} that do not depend on the data that was sent.

The main point for CM-DSS is that the expectation of the main contribution to the data recovery, $\eta_1(s_m)$, will be nonzero with independence of K when $\lambda_{1,m,k}$ has a coherence time in the order of or larger than T_c.

A. Derivation of the CM-DSS BER expression

Now that we have characterized D_m for the two-ray model as a RV under suitable hypothesis, following (20), we may calculate the bit error probability assuming s_m and s_{m-1} are *i.i.d.* binary sequences,

$$\begin{aligned}&Pr\left(\hat{s}_m\neq s_m\,|\boldsymbol{\lambda}_1,\boldsymbol{\lambda}_2\right)=\\&=\tfrac{1}{4}\sum_{s_m=\pm1}\sum_{s_{m-1}=\pm1}Pr\left(\hat{s}_m\neq s_m\,|s_m,s_{m-1},\boldsymbol{\lambda}_1,\boldsymbol{\lambda}_2\right),\end{aligned}\tag{25}$$

where

$$\begin{aligned}&Pr\left(\hat{s}_m\neq s_m\,|s_m,s_{m-1},\boldsymbol{\lambda}_1,\boldsymbol{\lambda}_2\right)=\\&=\tfrac{1}{2}\mathrm{erfc}\left(\tfrac{s_m\cdot\eta_{D_m}(s_m,s_{m-1})}{\sqrt{2}\sigma_{D_m}(s_m,s_{m-1})}\right).\end{aligned}\tag{26}$$

The unconditional bit error probability P_b can thus be calculated as

$$P_b=\mathrm{E}_{\boldsymbol{\lambda}_1,\boldsymbol{\lambda}_2}\left[Pr\left(\hat{s}_m\neq s_m\,|\boldsymbol{\lambda}_1,\boldsymbol{\lambda}_2\right)\right].\tag{27}$$

This requires calculating

$$\mathrm{E}_{\boldsymbol{\lambda}_1,\boldsymbol{\lambda}_2}\left[\mathrm{erfc}\left(\frac{s_m\cdot\eta_{D_m}(s_m,s_{m-1})}{\sqrt{2}\sigma_{D_m}(s_m,s_{m-1})}\right)\right],\tag{28}$$

which can only be done numerically: the mean and variance of D_m depend in a complex way on $\boldsymbol{\lambda}_1$ and $\boldsymbol{\lambda}_2$. The numerical evaluation of (27) based on the characterization of the D_m RV constitutes the analytical BER for the two-ray case and is used as such in Section IV. Furthermore, a simplified bound based on its analysis is derived and may be applied for the general $L\geq 2$ case.

B. Case studies for the two-ray model

We now address the analysis of the previous expressions under different situations. The objective is to properly characterize the limits within which a CM-DSS system is useful. The correct basis for the numerical evaluation of (27) is provided. Cases where no spreading sequence $x_{m,l}$ is used, just assuming $x_{m,l}=1$, are also compared against setups using a spreading sequence. In practice, a spreading sequence is not strictly required for the setup to work as may be inferred from the expressions of η_{D_m} and $\sigma_{D_m}^2$: the main contributions to data recovery $\eta_1(s_m)$ (36), and $\eta_7(s_m)$ (44)—d_2 even— and $\eta_{10}(s_m)$ (53)—d_2 odd—, are fully dependent on the evolution of the fading gains. Given the scope of the article, focused on improving DCSK, the spreading sequence used in the corresponding tests is based on the Chebyshev map [37]

$$x_n=1-2\cdot x_{n-1}^2,\tag{29}$$

normalized to unit power and zero mean. This is one of the preferred choices for DCSK systems given its properties

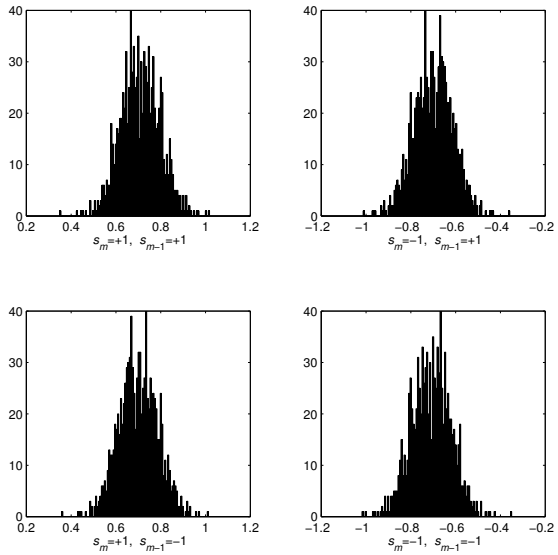

Fig. 4. Histograms of $\eta_{D_m}(s_m, s_{m-1})$ for $\beta = 100$, $K = 0$, $d_2 = 4$, $N_{\lambda_1} = 1$, $N_{\lambda_2} = 1$, $G_2 = G_1 - 3$ and spreading sequence (1000 runs).

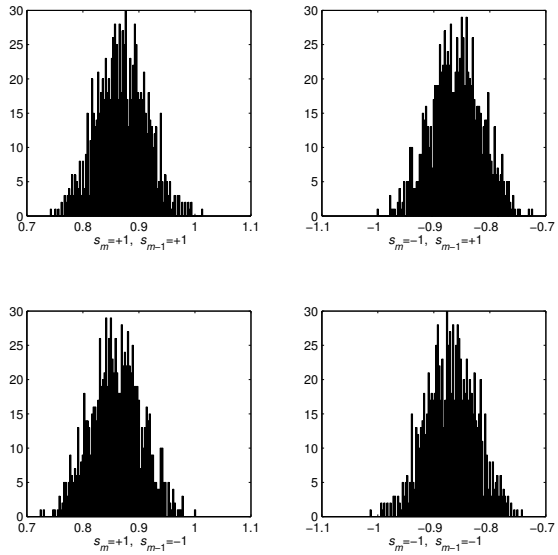

Fig. 5. Histograms of $\eta_{D_m}(s_m, s_{m-1})$ for $\beta = 100$, $K = 5$, $d_2 = 4$, $N_{\lambda_1} = 1$, $N_{\lambda_2} = 1$, $G_2 = G_1 - 3$ and no spreading sequence (1000 runs).

for LPI and anti-jamming. Note that even when a spreading sequence is not used, the waveform is still a spread one.

Let's examine the case with $d_2 << \beta$ even. The mean η_{D_m} has two main contributions to data recovery: from the first path (36) and from the second path (44). If the fading gains have normalized coherence times N_{λ_1} and N_{λ_2} much smaller than 1, these terms will go to zero for $K \to 0$, and the error probability will tend to 0.5. This has to do with the fact that the expected value of η_{D_m} turns out to be $\mathrm{E}[\eta_{D_m}(s_m, s'_m)] \approx s_m \cdot (R_{\lambda_1}[1] + R_{\lambda_2}[1])$. Some power may be recovered along each path when the normalized coherence time is in the order of 1 and larger, since in (8) we have $J_0(2\pi f_{d_l} T_c) = 0.7078$ for $N_{\lambda_l} = 1$.

The terms (39) to (42) depend on the crosscorrelation of the fading gains along the two paths, and they will be negligible when the spreading factor is large enough. The term (43) is an interference term depending on the previous symbol which may contribute significantly to η_{D_m} when the delay is large with respect to β.

In the accompanying figures, $G_1 = 20 \cdot \log_{10}(g_1)$ and $G_2 = 20 \cdot \log_{10}(g_2)$ represent the power gains, in dB, along the respective paths. $G_2 = G_1 - A$ means that the second path power is A dB below the power of the first one, under the constraint $g_1^2 + g_2^2 = 1$.

In Fig. 4, we have depicted a case with a spreading sequence, and where $K = 0$, $N_{\lambda_1} = 1$ and $N_{\lambda_2} = 1$. If the interference terms are negligible as mentioned above, the expected value for the mean results $\mathrm{E}[\eta_{D_m}(s_m, s'_m)] \approx s_m \cdot 0.7078$, in accordance with the histograms. Though not shown, the histograms without a spreading sequence are qualitatively and quantitatively identical. For higher normalized coherence times, the expected value for η_{D_m} will be higher, since $J_0(2\pi 9/(16\pi N_{\lambda_l}))$ is a growing function for growing N_{λ_l}.

Compare the former figure with Fig. 5, where now $K = 5$: the presence of a LOS component leads to a higher expected value for $\eta_{Dm}(s_m, s_{m-1})$ of approximately $s_m \cdot 0.87$. The worst situation would be for very small coherence times and no LOS, when $N_{\lambda_1} \to 0$, $N_{\lambda_2} \to 0$, since $J_0(\infty) = 0$: the fading coefficients will be fully uncorrelated along both paths, and $\mathrm{E}[\eta_{D_m}(s_m, s'_m)] = 0$. Note how for $K = 0$ and a fast fading with normalized coherence times of around $N_{\lambda_1} = N_{\lambda_2} = 1$, some power can still be recovered, as opposed to the DCSK case. In this situation, the chip-level correlation at the receiver is performed after β chip periods, and the fading coefficients will be fully uncorrelated unless the normalized coherence time is $N_{\lambda_l} \approx \beta$.

By looking into the contributions to the variance of D_m, and taking into account the mutual uncorrelation of both fading processes, we may conclude that the expected value for $\sigma^2_{D_m}$, for large β, $N_{\lambda_1} << \beta$, $N_{\lambda_2} << \beta$, will tend to

$$\mathrm{E}\left[\sigma^2_{D_m}\right] \approx 2\frac{\sigma^4}{\beta} + 2\frac{\sigma_n^2}{\beta}\left(\mathrm{E}\left[|\lambda_1|^2\right] + \mathrm{E}\left[|\lambda_2|^2\right]\right) = = 2\frac{\sigma_n^2}{\beta}\left(\sigma_n^2 + 1\right). \quad (30)$$

This approximation also holds when using a normalized spreading sequence, uncorrelated and independent from the fading, and with independence of the data symbol values. This will be reflected in the BER plots in the following way: the slope of the BER curves with same spreading factor β will be very similar for different setups (different parameter values, including K, G_1, G_2), since σ_n^2 only depends on E_b/N_0 and β. On the other hand, η_{D_m} will determine a shift in the BER curves reflecting the setup differences, given that its expected value depends on K, N_{λ_l} and g_l.

In Fig. 6, we can see the histograms for 1000 runs of the RVs representing $\sigma^2_{D_m}(s_m, s_{m-1})$, without a spreading sequence (the result with a spreading sequence, not shown,

is the same). It is to be noted that approximation (30) yields as expected a value of $\mathrm{E}\left[\sigma^2_{\mathrm{D_m}}\right] \approx 0.04$, irrespective of the data sent. The characterization of the variance or the mean of D_m with the help of their expected values may be useful, but this will be accurate only when the dispersion around the expected values is limited. When $N_{\lambda_1} \approx \beta$ and $N_{\lambda_2} \approx \beta$ for the same setup (histograms not shown), the dispersion of the RVs is much larger, and variance and mean can no longer be characterized by their expected values.

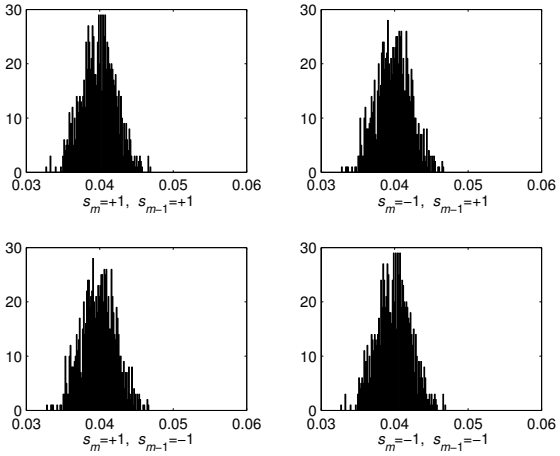

Fig. 6. Histograms of $\sigma^2_{D_m}(s_m, s_{m-1})$ for $E_b/N_0 = 20$ dB, $\beta = 100$, $K = 1$, $d_2 = 4$, $N_{\lambda_1} = 3$, $N_{\lambda_2} = 2$, $G_2 = G_1 - 3$ and no spreading sequence (1000 runs).

As shown in the figures, for even values of d_2 there seems to be no significant difference in adding a spreading sequence from the point of view of data recovery. This will be further highlighted in Section IV where we compare simulation results against their corresponding bounds. It is as well interesting to note that the influence of K will be relatively small when the other parameters remain constant, as could be deduced from (36): the value of the main data recovery term will largely depend on the power of the first path, g_1^2.

However, when d_2 is odd, there arise some interesting features. It is easy to demonstrate that approximation (30) for the variance holds, and that the interference terms in η_{D_m} containing the cross-product of channel gains across the two paths will also become negligible if d_2 is small with respect to β. The trends mentioned for the case with d_2 even respecting the contribution of (36) will exactly be the same. However, the possible data recovery from the second path, contained in term (53), poses a problem when a spreading sequence is added. Even when the expected value of $\lambda^*_{2,m,2j-2\beta_d+1} \cdot \lambda_{2,m,2(j-\beta_d+1)}$ is not null, when weighted by $x^*_{m,j-\beta_d} \cdot x_{m,j-\beta_d+1}$, the result would go to 0.

This effect can be clearly seen in Fig. 7. Note how in this case the contribution of the second path is completely wiped out, leading to an expected value of roughly $s_m \cdot R_{\lambda_1}[1] \approx s_m \cdot 0.6145$, instead of $s_m \cdot 0.9224$. Therefore, as shown in the accompanying figures, when d_2 is odd, it may be convenient not to use a spreading sequence, unless mandatory (i.e. when LPI is needed, or similarly jamming and interference resistance). In this latter case, some measures should be implemented to counteract, compensate or just take into account a sudden BER degradation arising from a possible change in the delay profile of the two paths. The consequences in terms of BER will be shown in Section IV.

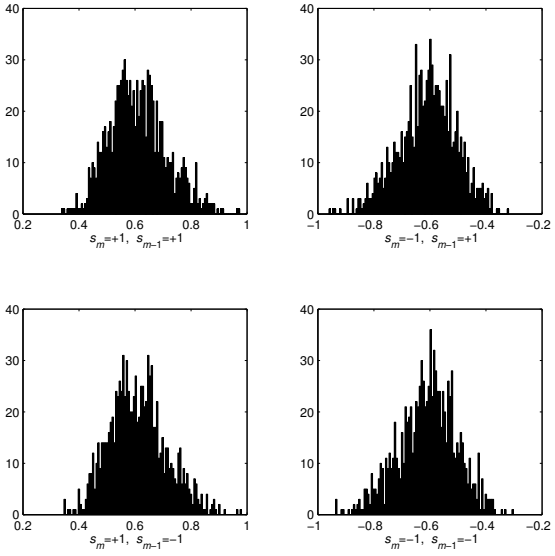

Fig. 7. Histograms of $\eta_{D_m}(s_m, s_{m-1})$ for $\beta = 100$, $K = 0$, $d_2 = 3$, $N_{\lambda_1} = 2$, $N_{\lambda_2} = 2$, $G_2 = G_1 - 3$ and spreading sequence (1000 runs).

All the cases and figures seen so far show that the interference from the previous bit is negligible, as may be inferred by the invariance of the histograms with respect to $s_{m-1} = \pm 1$. This holds so long as $d_2 << \beta$. When d_2 is a significant fraction of β, it may be shown that $\eta_{D_m}(s_m, s_{m-1})$ clearly suffers from the intererence of s_{m-1}. The behavior of variance $\sigma^2_{D_m}(s_m, s_{m-1})$ does not change overall: the effects of the data values are negligible so long as λ_1 and λ_2 remain uncorrelated, and $\beta >> 1$.

The previous analysis has shown the possibilities and limitations of the system. In order for the CM-DSS scheme to be practical, some properties should be guaranteed:

- The delay should be $d_2 << \beta$, so that the interference of the previous symbol along the second path is limited.
- Coherence times have to be in the order of T_c, so that $N_{\lambda_1} \geq 1$ or $N_{\lambda_2} \geq 1$: in this case, signal power and subsequent data recovery may be performed successfully, from the first and/or second path.
- If a spreading sequence is used, the second path delay d_2 should be guaranteed not to be an odd number of chips in order to have proper frame alignment.

This analysis has also shown that, when $\beta >> 1$, $N_{\lambda_1} << \beta$, $N_{\lambda_2} << \beta$, we may use approximation (30) for $\sigma^2_{D_m}(s_m, s_{m-1})$, and the following one for the mean when d_2 is even

$$\eta'_{D_m} \approx s_m \left(R_{\lambda_1}[1] + R_{\lambda_2}[1]\right). \tag{31}$$

Under the hypothesis that $d_i << \beta$ and $N_{\lambda_i} << \beta$ for all i,

this expression may be escalated for $L \geq 2$ paths

$$\eta'_{D_m} \approx s_m \sum_{i=1}^{L} R_{\lambda_i}[1]. \tag{32}$$

thus leading straightforwardly to a more general simplified bound

$$P_b \approx \frac{1}{2}\mathrm{erfc}\left(\frac{\sum_{i=1}^{L} R_{\lambda_i}[1]}{\sqrt{4\sigma_n^2(\sigma_n^2+1)/\beta}}\right). \tag{33}$$

This bound uses expected values to represent quantities that in practice are RVs. When d_i is odd, (32) is valid *only* if no spreading sequence is used. Otherwise, (33) may still be valid with the following new definition for η'_{D_m}

$$\eta'_{D_m} \approx s_m \sum_{i=1}^{L} (1 - d_i \bmod 2) R_{\lambda_l}[1]. \tag{34}$$

In the following section, all these points are illustrated with the help of BER simulations. The results of the proposed system are compared with those of other systems like the ones based on DSS. More specifically and in accordance with the scope of this article, the focus is on DCSK- and CM-DCSK-based systems although the developments presented in this section are completely general.

IV. Simulation results and discussions

In this section the BER performance of CM-DCSK is evaluated and compared with that of the DCSK setup. The chaotic spreading sequence used is based on the Chebyshev map [37], as in the previous section. The numerical evaluation of the analytic result of (27) is calculated based on $10,000$ runs of the D_m RV. Almost all of the results throughout this section are for $d_2 \ll \beta$, meaning that the intersymbol interference is largely negligible. Furthermore and as shown with the analysis presented in the previous section, this also means that effects remarked in the related plots solely have to do with the profile of the multipath channel.

Fig. 8 illustrates some performance results for both CM-DCSK and DCSK schemes in the two-path channel model. The figure shows tight accordance between the numerically evaluated analytical result of (27) and the corresponding simulations, thus validating the approach. The approximate bound of (33) captures the trend of the curves. The simplified bound gives thus a good approximation for E_b/N_0 below 20 dB, where the noise is able to mask the rest of effects on the mean and variance of D_m: the expectaction of $\sigma^2_{D_m}$ (30) is large with respect to the variations caused by the multipath fading channel. Therefore, if a setup reaches a target BER of 10^{-5} beyond 20 dB (cases where the power of some of the main paths is lost and η_{D_m} takes low values), it is almost certain that the simplified bound would not be very tight for the BER ranges of practical interest when $\beta = 100$. For larger values of β, the approximation of (33) will keep its relative tightness for a larger range of E_b/N_0, because said variations become relatively lower. As expected from the previous analysis, CM-DCSK performs better as N_{λ_1} grows. On the other hand, conventional DCSK always delivers the same bad performance as $N_{\lambda_1} \ll \beta$, $N_{\lambda_2} \ll \beta$. Note that, even in this case, some power is still recovered due to the presence of a LOS path ($K = 1$).

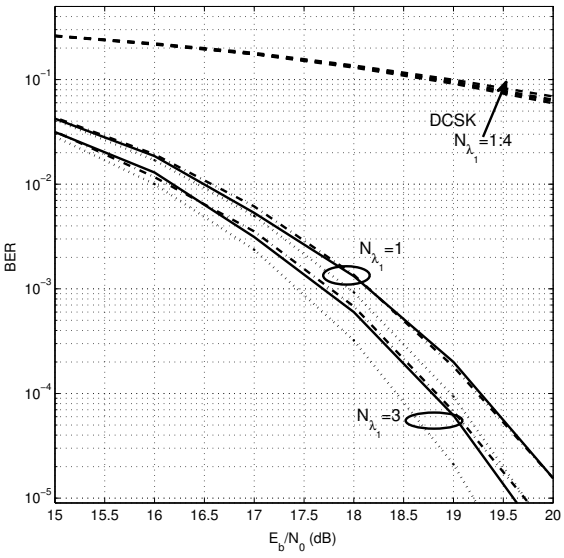

Fig. 8. CM-DCSK simulation results (continuous lines), (27) numerically evaluated (dash-dotted lines), (33) simplified bound (dotted lines), and simulation results for DCSK (dashed lines), for different N_{λ_1}. $\beta = 100$, $K = 1$, $N_{\lambda_2} = 3$, $d_2 = 2$, $G_2 = G_1 - 3$.

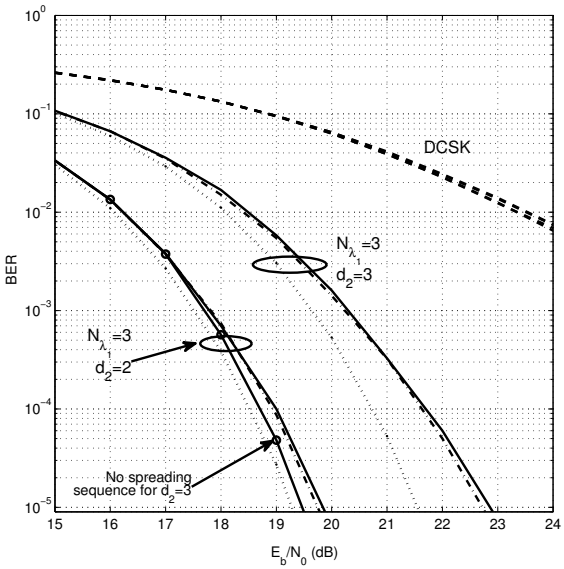

Fig. 9. CM-DCSK simulation results (continuous lines), (27) numerically evaluated (dash-dotted lines), (33) simplified bound (dotted lines), and simulation results for DCSK (dashed lines), for different d_2. $\beta = 100$, $K = 1$, $N_{\lambda_1} = 3$, $N_{\lambda_2} = 2$, $G_2 = G_1 - 3$. 'o': case $d_2 = 3$ without a spreading sequence.

Fig. 9 shows the effect of d_2 on the BER performance of the proposed system over the two-path fading channel. As may be observed, when d_2 is odd and a spreading sequence is used, there is a performance degradation due to the fact that no power is recovered from the second path. See how this does not happen when no spreading sequence is used. In a normal scenario, a spreading sequence has to be used regardless of the characteristics of the delay profile

of the channel, because in a non-coherent system like this LPI is required as well as anti-jamming and anti-interference properties. This undesirable effect of d_2 may be overcome by appropriately managing the bit and chip periods, under a pre-established protocol. A full CSI would still not be needed as a basic characterization of the channel profile would suffice. As previously seen, DCSK cannot offer good performance in any case. Note that, again, the numerical evaluation of the analytical BER captures the behavior of the experimental data: the advantage of the former from the point of view of the analysis and design is that the calculations involved are less time and resource consuming than the ones usually devoted to a standard simulation. Regarding the simplified bound (33), it keeps its mentioned relative tightness within the mentioned E_b/N_0-BER limits.

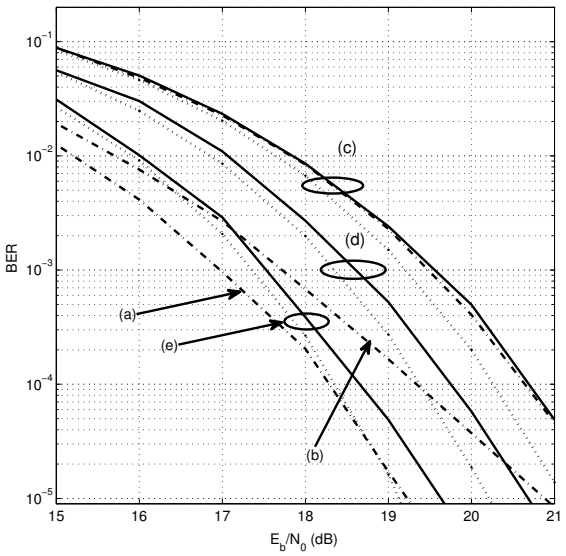

Fig. 10. CM-DCSK simulation results (continuous lines), (27) numerically evaluated (dash-dotted lines), (33) simplified bound (dotted lines) for other scenarios. (a) $K = 1$, $\beta = 50$, $d_2 = 2$, $N_{\lambda_1} = 2$, $N_{\lambda_2} = 4$, $G_2 = G_1 - 3$. (b) Same as (a), except $d_2 = 20$. (c) CM-DSS with random sequence, for $K = 0$, $\beta = 100$, $d_2 = 2$, $N_{\lambda_1} = 1$, $N_{\lambda_2} = 1$, $G_2 = G_1 - 3$. (d) CM-DCSK results for 3 paths, $K = 1$, $\beta = 100$, $d_l = 0, 2, 3$, $N_{\lambda_l} = 2, 3, 3$, $G_2 = G_1 - 3$, $G_3 = G_1 - 6$. (e) Results for 4 paths, $K = 20$, $\beta = 100$, $d_l = 0, 2, 4, 6$, $N_{\lambda_l} = 2, 4, 6, 8$, $G_2 = G_1 - 3$, $G_3 = G_1 - 6$, $G_4 = G_1 - 9$.

Fig. 10 illustrates performance for other scenarios. When d_2 is in the order of magnitude of β (case (b)), the effect of intersymbol interference translates into a degraded BER in comparison to $d_2 \ll \beta$ (case (a)). This can be overcome by increasing the spreading factor: this feature can be controlled through the same basic protocol of channel profile identification as mentioned for the control of d_2 odd. The simplified bound (not shown) is the same for cases (a) and (b), and is totally inaccurate for $d_2 \approx \beta$. A CM-DSS case is also represented with another kind of spreading sequence, namely a random one (case (c)). It can be seen that the results are comparable, and expressions (27) and (33) can still be applied under the same conditions. The corresponding results with a Chebyshev sequence (not shown) are the same. Nevertheless, the scope here focuses mainly on DCSK and its improvement for the continuous-mobility scenario, since the chaotic spreading sequences may be preferred due to their LPI and correlation properties [9], [10].

The figure also shows what happens with a larger number of paths with decreasing power (cases (d)-(e)), where (27) has logically not been depicted. The results follow the same trends seen with the two-path model. The results in (d) are poorer than other cases because the power in the third path is lost ($d_3 = 3$). The results in (e) for 4 paths is better because the first path is clearly dominant with a high LOS component. Note how the simplified bound (33), generalized to $L > 2$ paths, follows the detected trends, confirming that it can be useful in the appropriate regions of interest.

V. Conclusions

A continuous-mobility differential spread-spectrum non-coherent system has been proposed in this paper, with direct application to the well known DCSK setup. This new system aims at enhancing the adaptability of the receiver when the channel is affected by fast fading without the need of a thorough channel estimation, which is costly and time consuming. To reach this target, a new frame signal was proposed where each reference sample is followed by its corresponding data carrier sample. This modification of the system design may also help in reducing the hardware complexity by avoiding the use of long wideband delay lines.

The proposed system was shown to significantly improve performance under fast fading, while retaining the desirable non-coherent nature of the scheme. The analysis performed has led to the establishment of an analytical expression for the two-path fading model. Its numerical evaluation has been validated to be very accurate when confronted to the simulation results. This numerical evaluation is much easier and less resource consuming than the typical simulation work. Additionally, a simplified bound with general applicability to a multipath channel has been derived, and was shown to be tight enough for fast evaluation and characterization of CM-DSS systems.

The obtained results highlight the importance of the CM-DSS design to exploit the time diversity of wireless channels. In order to do this, we have to make sure that the delay profile of the multipath components keep some key characteristics: low delay values compared to the bit frame duration, and even delay values (in number of chips) for the paths with highest power. While this implies that some on-the-go elementary channel identification protocol has to take place in order to correctly adjust the bit and chip rates in the continuous-mobility scenario, this does not require full CSI.

The application of all these principles to DCSK in the form of CM-DCSK has shown a great performance enhancement compared to conventional DCSK. Considering the need and demand for future low rate continuous wireless non-coherent communications with minimal complexity, typical for the envisioned internet of things (IoT) pervading needs, the proposed CM-DSS system seems to be a promising alternative.

APPENDIX A
DERIVATION OF MEAN AND VARIANCE FOR EVEN DELAYS

According to the expression given for the decision variable D_m (18), we may decompose it into several contributions, by defining $\beta_d = d_2/2$, following:

- $\frac{1}{\beta}\Re\left[\sum_{j=0}^{\beta-1} n_{2j}^* n_{2j+1}\right]$, which, for $\beta >> 1$, by virtue of the Central Limit Theorem, is well approximated as a zero-mean Gaussian random variable with variance

$$\sigma_1^2 = \frac{2\sigma_n^4}{\beta}. \tag{35}$$

- $\frac{1}{\beta}\Re\left[\sum_{j=0}^{\beta-1} \left(\lambda_{1,m,2j} e_{m,2j}\right)^* \left(\lambda_{1,m,2j+1} e_{m,2j+1}\right)\right]$, which is the main term contributing to the information recovery. It can be simplified to

$$\eta_1\left(s_m\right) = \frac{s_m}{\beta}\sum_{j=0}^{\beta-1} |x_{m,j}|^2 \Re\left[\lambda_{1,m,2j}^* \lambda_{1,m,2j+1}\right] \tag{36}$$

  The expectation $\mathrm{E}[\cdot]$ of this random variable is nonzero when $\lambda_{1,m,k}$ is highly correlated during a number of several chip intervals, thus allowing for the information recovery, in contrast to the DSS case.
- The term

$$\begin{aligned}\frac{1}{\beta}\Re\Bigg[\sum_{j=0}^{\beta_d-1} &\left(\lambda_{1,m,2j} e_{m,2j} + \right.\\ &+\lambda_{2,m-1,2j-d_2+2\beta} e_{m-1,2j-d_2+2\beta}\big)^* \cdot n_{2j+1} + \\ &+\sum_{j=\beta_d}^{\beta-1}\left(\lambda_{1,m,2j} e_{m,2j} + \right.\\ &\left.\left.+\lambda_{2,m,2j-d_2} e_{m,2j-d_2}\right)^* \cdot n_{2j+1}\Bigg]\end{aligned}$$

  is a zero-mean Gaussian random variable with variance

$$\begin{aligned}\sigma_2^2 = \frac{\sigma_n^2}{\beta^2}\Bigg[&\sum_{j=0}^{\beta_d-1} |\lambda_{1,m,2j}\cdot x_{m,j} + \\ &+\lambda_{2,m-1,2j-2\beta_d+2\beta}\cdot x_{m-1,j-\beta_d+\beta}|^2 + \\ &+\sum_{j=\beta_d}^{\beta-1}|\lambda_{1,m,2j}\cdot x_{m,j} + \\ &+\lambda_{2,m,2j-2\beta_d} x_{m,j-\beta_d}|^2\Bigg]\end{aligned} \tag{37}$$

- The term

$$\begin{aligned}\frac{1}{\beta}\Re\Bigg[&\sum_{j=0}^{\beta_d-1} n_{2j}^*\cdot\left(\lambda_{1,m,2j+1} e_{m,2j+1} + \right.\\ &+\lambda_{2,m-1,2j+1-d_2+2\beta} e_{m-1,2j+1-d_2+2\beta}\big) + \\ &+\sum_{j=\beta_d}^{\beta-1} n_{2j}^*\cdot\left(\lambda_{1,m,2j+1} e_{m,2j+1} + \right.\\ &\left.\left.+\lambda_{2,m,2j+1-d_2} e_{m,2j+1-d_2}\right)\Bigg]\end{aligned}$$

  is a zero-mean Gaussian random variable with variance

$$\begin{aligned}\sigma_3^2\left(s_m, s_{m-1}\right) = \frac{\sigma_n^2}{\beta^2}\cdot\\ \cdot\Bigg[\sum_{j=0}^{\beta_d-1}&|\lambda_{1,m,2j+1}\cdot s_m\cdot x_{m,j} + \\ &+\lambda_{2,m-1,2j+1-2\beta_d+2\beta}\cdot s_{m-1}\cdot x_{m-1,j-\beta_d+\beta}|^2 + \\ &+\sum_{j=\beta_d}^{\beta-1}|\lambda_{1,m,2j+1}\cdot x_{m,j} + \\ &\left.\lambda_{2,m,2j+1-2\beta_d}\cdot x_{m,j-\beta_d}|^2\right].\end{aligned} \tag{38}$$

- The term

$$\begin{aligned}\frac{1}{\beta}\Re\Bigg[&\sum_{j=0}^{\beta_d-1}\left(\lambda_{1,m,2j}\cdot e_{m,2j}\right)^*\cdot\\ &\left(\lambda_{2,m-1,2j+1-d_2+2\beta}\cdot e_{m-1,2j+1-d_2+2\beta}\right)\Bigg],\end{aligned}$$

  is an interference term from the previously transmitted symbol s_{m-1}, following

$$\begin{aligned}\eta_2(s_{m-1}) = \frac{s_{m-1}}{\beta}\Re\Bigg[&\sum_{j=0}^{\beta_d-1}\left(x_{m,j}^*\cdot x_{m-1,j-\beta_d+\beta}\right)\cdot\\ &\cdot\left(\lambda_{1,m,2j}^*\cdot\lambda_{2,m-1,2j+1-2\beta_d+2\beta}\right)\Bigg].\end{aligned} \tag{39}$$

- The term

$$\begin{aligned}\frac{1}{\beta}\Re\Bigg[&\sum_{j=\beta_d}^{\beta-1}\left(\lambda_{1,m,2j} e_{m,2j}\right)^*\cdot\\ &\cdot\left(\lambda_{2,m,2j+1-d_2} e_{m,2j+1-d_2}\right)\Bigg],\end{aligned}$$

  can be rewritten as

$$\begin{aligned}\eta_3(s_m) = \frac{s_m}{\beta}\Re\Bigg[&\sum_{j=\beta_d}^{\beta-1}\left(\lambda_{1,m,2j}^*\cdot\lambda_{2,m,2j+1-2\beta_d}\right)\cdot\\ &\cdot\left(x_{m,j}^*\cdot x_{m,j-\beta_d}\right)\Bigg],\end{aligned} \tag{40}$$

  and is an information recovery term.
- The term

$$\begin{aligned}\frac{1}{\beta}\Re\Bigg[&\sum_{j=0}^{\beta_d-1}\left(\lambda_{2,m-1,2j-d_2+2\beta}\cdot e_{m-1,2j-d_2+2\beta}\right)^*\cdot\\ &\cdot\left(\lambda_{1,m,2j+1}\cdot e_{m,2j+1}\right)\Bigg],\end{aligned}$$

  can be rewritten as

$$\begin{aligned}\eta_4(s_m) = \frac{s_m}{\beta}\Re\Bigg[&\sum_{j=0}^{\beta_d-1}\left(x_{m-1,j-\beta_d+\beta}^*\cdot x_{m,j}\right)\cdot\\ &\cdot\left(\lambda_{2,m-1,2j-2\beta_d+2\beta}^*\cdot\lambda_{1,m,2j+1}\right)\Bigg],\end{aligned} \tag{41}$$

  and results in an information recovery term.

- The term

$$\frac{1}{\beta}\Re\left[\sum_{j=\beta_d}^{\beta-1}\left(\lambda_{2,m,2j-d_2}\cdot e_{m,2j-d_2}\right)^*\cdot \cdot\left(\lambda_{1,m,2j+1}\cdot e_{m,2j+1}\right)\right],$$

can be rewritten as

$$\eta_5(s_m)=\frac{s_m}{\beta}\Re\left[\sum_{j=\beta_d}^{\beta-1}\left(\lambda^*_{2,m,2j-2\beta_d}\cdot\lambda_{1,m,2j+1}\right)\cdot \cdot\left(x^*_{m,j-\beta_d}\cdot x_{m,j}\right)\right], \quad (42)$$

which is an information recovery term.

- The term

$$\frac{1}{\beta}\Re\left[\sum_{j=0}^{\beta_d-1}\left(\lambda_{2,m-1,2j-d_2+2\beta}\cdot e_{m-1,2j-d_2+2\beta}\right)^*\cdot \cdot\left(\lambda_{2,m-1,2j+1-d_2+2\beta}\cdot e_{m-1,2j+1-d_2+2\beta}\right)\right],$$

can be rewritten as

$$\eta_6(s_{m-1})=\frac{s_{m-1}}{\beta}\sum_{j=0}^{\beta_d-1}\left|x_{m-1,j-\beta_d+\beta}\right|^2\cdot \cdot\Re\left[\left(\lambda^*_{2,m-1,2j-2\beta_d+2\beta}\cdot\lambda_{2,m-1,2j+1-\beta_d+2\beta}\right)\right], \quad (43)$$

which is an additional interference term.

- The term

$$\frac{1}{\beta}\Re\left[\sum_{j=\beta_d}^{\beta-1}\left(\lambda_{2,m,2j-d_2}\cdot e_{m,2j-d_2}\right)^*\cdot \cdot\left(\lambda_{2,m,2j+1-d_2}\cdot e_{m,2j+1-d_2}\right)\right],$$

can be rewritten as

$$\eta_7(s_m)=\frac{s_m}{\beta}\sum_{j=\beta_d}^{\beta-1}\left|x_{m,j-\beta_d}\right|^2\cdot \cdot\Re\left[\left(\lambda^*_{2,m,2j-2\beta_d}\cdot\lambda_{2,m,2j+1-2\beta_d}\right)\right], \quad (44)$$

which is another contribution to the data recovery.

Appendix B
Derivation of mean and variance for odd delays

When the delay of the second path is odd, and defining $\beta_d=(d_2+1)/2$, the decomposition of the decision variable D_m (18) turns into:

- $\eta_1(s_m)$ is the same as in the even delay case from Appendix A,
- σ_1^2 is also the same as in the previous case,

and we have another series of contributions to the mean of the equivalent Gaussian random variable, given straightfordwardly as:

$$\eta_2=\frac{1}{\beta}\Re\left[\sum_{j=0}^{\beta_d-2}\left(x^*_{m,j}\cdot x_{m-1,j-\beta_d+\beta+1}\right)\cdot \cdot\left(\lambda^*_{1,m,2j}\cdot\lambda_{2,m-1,2(j-\beta_d+\beta+1)}\right)\right], \quad (45)$$

$$\eta_3\left(s_{m-1},s_m\right)=\frac{s_{m-1}s_m}{\beta}\cdot \cdot\Re\left[\sum_{j=0}^{\beta_d-2}\left(x^*_{m-1,j-\beta_d+\beta}\cdot x_{m,j}\right)\cdot \cdot\left(\lambda^*_{2,m-1,2(j-\beta_d+\beta)+1}\cdot\lambda_{1,m,2j+1}\right)\right], \quad (46)$$

$$\eta_4\left(s_{m-1}\right)=\frac{s_{m-1}}{\beta}\cdot \quad (47)$$
$$\cdot\Re\left[\sum_{j=0}^{\beta_d-2}\left(x^*_{m-1,j-\beta_d+\beta}\cdot x_{m-1,j-\beta_d+\beta+1}\right)\cdot \cdot\left(\lambda^*_{2,m-1,2(j-\beta_d+\beta)+1}\cdot\lambda_{2,m-1,2(j-\beta_d+\beta+1)}\right)\right],$$

$$\eta_5=\frac{1}{\beta}\Re\left[\left(x^*_{m,\beta_d-1}\cdot x_{m,0}\right)\cdot \cdot\left(\lambda^*_{1,m,2(\beta_d-1)}\cdot\lambda_{2,m,0}\right)\right], \quad (48)$$

$$\eta_6\left(s_{m-1},s_m\right)=\frac{s_{m-1}s_m}{\beta}\Re\left[\left(x^*_{m-1,\beta-1}\cdot x_{m,\beta_d-1}\right)\cdot \cdot\left(\lambda^*_{2,m-1,2\beta-1}\cdot\lambda_{1,m,2\beta_d-1}\right)\right], \quad (49)$$

$$\eta_7\left(s_{m-1}\right)=\frac{s_{m-1}}{\beta}\Re\left[\left(x^*_{m-1,\beta-1}\cdot x_{m,0}\right)\cdot \cdot\left(\lambda^*_{2,m-1,2\beta-1}\cdot\lambda_{2,m,0}\right)\right], \quad (50)$$

$$\eta_8=\frac{1}{\beta}\Re\left[\sum_{j=\beta_d}^{\beta-1}\left(x^*_{m,j}\cdot x_{m,j-\beta_d+1}\right)\cdot \cdot\left(\lambda^*_{1,m,2j}\cdot\lambda_{2,m,2(j-\beta_d+1)}\right)\right], \quad (51)$$

$$\eta_9=\frac{1}{\beta}\Re\left[\sum_{j=\beta_d}^{\beta-1}\left(x^*_{m,j-\beta_d}\cdot x_{m,j}\right)\cdot \cdot\left(\lambda^*_{2,m,2j-2\beta_d+1}\cdot\lambda_{1,m,2j+1}\right)\right], \quad (52)$$

$$\eta_{10}\left(s_m\right)=\frac{s_m}{\beta}\Re\left[\sum_{j=\beta_d}^{\beta-1}\left(x^*_{m,j-\beta_d}\cdot x_{m,j-\beta_d+1}\right)\cdot \cdot\left(\lambda^*_{2,m,2j-2\beta_d+1}\cdot\lambda_{2,m,2(j-\beta_d+1)}\right)\right]. \quad (53)$$

On the other hand, the variance has other two terms:

$$\begin{aligned}\sigma_2^2\left(s_{m-1},s_m\right)=\frac{\sigma_n^2}{\beta^2}\sum_{j=0}^{\beta_d-2}&\left|\lambda_{1,m,2j}\cdot x_{m,j}+\right.\\&+\left.\lambda_{2,m-1,2(j-\beta_d+\beta)+1}\cdot s_{m-1}\cdot x_{m-1,j-\beta_d+\beta}\right|^2+\\&+\frac{\sigma_n^2}{\beta^2}\left|\lambda_{1,m,2(\beta_d-1)}\cdot x_{m,\beta_d-1}+\right.\\&+\left.\lambda_{2,m-1,2\beta-1}\cdot s_{m-1}\cdot x_{m-1,\beta-1}\right|^2+\\&+\frac{\sigma_n^2}{\beta^2}\sum_{j=\beta_d}^{\beta-1}\left|\lambda_{1,m,2j}\cdot x_{m,j}+\right.\\&+\left.\lambda_{2,m,2(j-\beta_d)+1}\cdot s_m\cdot x_{m,j-\beta_d}\right|^2,\end{aligned} \quad (54)$$

$$\sigma_3^2(s_m) = \frac{\sigma_n^2}{\beta^2}\sum_{j=0}^{\beta_d-2}\left|\lambda_{1,m,2j+1}\cdot s_m\cdot x_{m,j}+\right.$$
$$\left.+\,\lambda_{2,m-1,2(j-\beta_d+\beta+1)}\cdot x_{m-1,j-\beta_d+\beta+1}\right|^2+$$
$$+\frac{\sigma_n^2}{\beta^2}\left|\lambda_{1,m,2\beta_d-1}\cdot s_m\cdot x_{m,\beta_d-1}+\right.$$
$$\left.+\,\lambda_{2,m,0}\cdot x_{m,0}\right|^2+$$
$$+\frac{\sigma_n^2}{\beta^2}\sum_{j=\beta_d}^{\beta-1}\left|\lambda_{1,m,2j+1}\cdot s_m\cdot x_{m,j}+\right. \quad (55)$$
$$\left.+\,\lambda_{2,m,2(j-\beta_d+1)}\cdot x_{m,j-\beta_d+1}\right|^2.$$

ACKNOWLEDGMENT

The authors acknowledge financial support from the NSERC discovery grant $435243-2013$.

REFERENCES

[1] S. Vitali, R. Rovatti, and G. Setti, "Improving PA efficiency by chaos-based spreading in multicarrier DS-CDMA systems," in *Proc. IEEE Int. Symp. Circuits and Syst. (ISCAS)*, May 2006, pp. 4 pp.–1198.

[2] R. Vali, S. Berber, and S. K. Nguang, "Accurate Derivation of Chaos-Based Acquisition Performance in a Fading Channel," *IEEE Trans. Wireless Commun.*, vol. 11, no. 2, pp. 722–731, February 2012.

[3] Y. Fang, J. Xu, L. Wang, and G. Chen, "Performance of MIMO relay DCSK-CD systems over Nakagami fading channels," *IEEE Trans. Circuits Syst. I*, vol. 60, pp. 1–11, March 2013.

[4] Y. Fang, L. Wang, and G. Chen, "Performance of a multiple-access DCSK-CC system over Nakagami-m fading channels," in *Proc. IEEE Int. Symp. Circuits and Syst. (ISCAS)*, 2013.

[5] W. Xu, L. Wang, and G. Chen, "Performance of DCSK Cooperative Communication Systems Over Multipath Fading Channels," *IEEE Trans. Circuits Syst. I*, vol. 58, no. 1, pp. 196–204, January 2011.

[6] C.-C. Chong and S. K. Yong, "UWB Direct Chaotic Communication Technology for Low-Rate WPAN Applications," *IEEE Trans. Veh. Technol.*, vol. 57, no. 3, pp. 1527–1536, May 2008.

[7] G. Kaddoum, F.-D. Richardson, and F. Gagnon, "Design and Analysis of a Multi-Carrier Differential Chaos Shift Keying Communication System," *IEEE Trans. Commun.*, vol. 61, no. 8, pp. 3281–3291, 2013.

[8] F. C. M. Lau and C. K. Tse, *Chaos-Based Digital Communication Systems*. Springer-Verlag, 2003.

[9] J. Yu and Y.-D. Yao, "Detection performance of chaotic spreading LPI waveforms," *IEEE Trans. Wireless Commun.*, vol. 4, no. 2, pp. 390–396, March 2005.

[10] F. Zhu, J. Xu, and M. Chen, "The Combination of High-Gain Sliding Mode Observers Used as Receivers in Secure Communication," *IEEE Trans. Circuits Syst. I*, vol. 59, no. 11, pp. 2702–2712, 2012.

[11] S. Manoharan and V. Bhaskar, "PN codes versus chaotic codes: Performance comparison in a Gaussian approximated wideband CDMA system over Weibull fading channels," *J. Franklin Institute*, 2014.

[12] L. Wang, C. Zhang, and G. Chen, "Performance of an SIMO FM-DCSK Communication System," *IEEE Trans. Circuits Syst. II*, vol. 55, no. 5, pp. 457–461, May 2008.

[13] H.-P. Ren, M. S. Baptista, and C. Grebogi, "Wireless Communication with Chaos," *Phys. Rev. Lett.*, vol. 110, p. 184101, Apr 2013.

[14] M. P. Kennedy, G. Kolumbán, G. Kis, and Z. Jákó, "Performance evaluation of FM-DCSK modulation in multipath environments," *IEEE Trans. Circuits Syst. I*, vol. 47, no. 12, pp. 1702–1711, Dec 2000.

[15] J. Schweizer and T. Schimming, "Symbolic dynamics for processing chaotic signal. II. Communication and coding," *IEEE Trans. Circuits Syst. I*, vol. 48, no. 11, pp. 1283–1295, Nov 2001.

[16] P. Chen, L. Wang, and F. Lau, "One Analog STBC-DCSK Transmission Scheme not Requiring Channel State Information," *IEEE Trans. Circuits Syst. I*, vol. 60, no. 4, pp. 1027–1037, 2013.

[17] G. Kaddoum, E. Soujeri, C. Arcila, and K. Eshteiwi, "I-DCSK: An Improved Noncoherent Communication System Architecture," *IEEE Trans. Circuits Syst. II*, vol. 62, no. 9, pp. 901–905, Sept 2015.

[18] Y. Fang, L. Wang, P. Chen, J. Xu, G. Chen, and W. Xu, "Design and Analysis of a DCSK-ARQ/CARQ System Over Multipath Fading Channels," *IEEE Trans. Circuits Syst. I*, vol. 62, no. 6, pp. 1637–1647, June 2015.

[19] N. X. Quyen, V. V. Yem, and T. Q. Duong, "Design and analysis of a spread-spectrum communication system with chaos-based variation of both phase-coded carrier and spreading factor," *IET Commun.*, vol. 9, no. 12, pp. 1466–1473, 2015.

[20] G. Kaddoum, "Design and Performance Analysis of a Multiuser OFDM Based Differential Chaos Shift Keying Communication System," *IEEE Trans. Commun.*, vol. 64, no. 1, pp. 249–260, Jan 2016.

[21] G. Kaddoum, E. Soujeri, and Y. Nijsure, "Design of a Short Reference Noncoherent Chaos-Based Communication Systems," *IEEE Trans. Commun.*, vol. 64, no. 2, pp. 680–689, Feb 2016.

[22] H. Yang, W. K. S. Tang, G. Chen, and G. P. Jiang, "System Design and Performance Analysis of Orthogonal Multi-Level Differential Chaos Shift Keying Modulation Scheme," *IEEE Trans. Circuits Syst. I*, vol. 63, no. 1, pp. 146–156, Jan 2016.

[23] Z. Zhou, T. Zhou, and J. Wang, "Performance of Multiple-Access DCSK Communication over a Multipath Fading Channel with Delay Spread," *Circuits, Syst. & Signal Process.*, vol. 27, no. 4, pp. 507–518, 2008.

[24] G. Kaddoum, J. Olivain, G. Beaufort Samson, P. Giard, and F. Gagnon, "Implementation of a Differential Chaos Shift Keying communication system in GNU Radio," in *Proc. Int. Symp. Wireless Commun. Syst. (ISWCS)*, 2012, pp. 934–938.

[25] G. Kaddoum, F. Gagnon, P. Charge, and D. Roviras, "A Generalized BER Prediction Method for Differential Chaos Shift Keying System Through Different Communication Channels," *Wireless Personal Commun.*, vol. 64, pp. 425–437, 2012.

[26] J. Xu, W. Xu, L. Wang, and G. Chen, "Design and simulation of a cooperative communication system based on DCSK/FM-DCSK," in *Proc. IEEE Int. Symp. Circuits and Syst. (ISCAS)*, June 2010, pp. 2454–2457.

[27] S. Wang and X. Wang, "M-DCSK-based Chaotic Communications in MIMO Multipath Channels With No Channel State Information," *IEEE Trans. Circuits Syst. II*, vol. 57, no. 12, pp. 1001–1005, Dec 2010.

[28] Y. Xia, C. K. Tse, and F. C. M. Lau, "Performance of differential chaos-shift-keying digital communication systems over a multipath fading channel with delay spread," *IEEE Trans. Circuits Syst. II*, vol. 51, pp. 680–684, 2004.

[29] W. K. Xu, L. Wang, and K. G., "A Novel Differential Chaos Shift Keying Modulation Scheme," *Int. J. Bifurcation and Chaos*, vol. 21, no. 03, pp. 799–814, 2011.

[30] G. Kaddoum and F. Gagnon, "Design of a High-Data-Rate Differential Chaos-Shift Keying System," *IEEE Trans. Circuits Syst. II*, vol. 59, no. 99, pp. 1–5, July 2012.

[31] F. Lau, K. Cheong, and C. Tse, "Permutation-based DCSK and multiple-access DCSK systems," *IEEE Trans. Circuits Syst. I*, vol. 50, pp. 733–742, 2003.

[32] W. Tam, F. Lau, and C. Tse, "Generalized correlation-delay-shift-keying scheme for noncoherent chaos-based communication systems," in *Proc. IEEE Int. Symp. Circuits and Syst. (ISCAS)*, vol. 4, May 2004, pp. IV–601–4 Vol.4.

[33] L. Wang, G. Cai, and G. R. Chen, "Design and Performance Analysis of a New Multiresolution M -Ary Differential Chaos Shift Keying Communication System," *IEEE Trans. Wireless Commun.*, vol. 14, no. 9, pp. 5197–5208, Sept 2015.

[34] G. Kaddoum, F. Gagnon, and F.-D. Richardson, "Design of a secure Multi-Carrier DCSK system," in *Proc. Int. Symp. on Wireless Commun. Syst. (ISWCS)*, Aug 2012, pp. 964–968.

[35] E. Biglieri, J. Proakis, and S. Shamai, "Fading Channels: Information-Theoretic and Communications Aspects," *IEEE Trans. Inf. Theory*, vol. 44, pp. 2619–2692, Oct. 1998.

[36] B. Sklar, "Rayleigh fading channels in mobile digital communication systems. I. Characterization," *IEEE Commun. Mag.*, vol. 35, no. 9, pp. 136–146, Sep 1997.

[37] K. Umeno and K. Kitayama, "Improvement of SNR with Chaotic Spreading Sequences for CDMA," in *Proc. IEEE Inf. Theory Workshop*, 1999, p. 106.

Francisco J. Escribano received his degree in Telecommunications Engineering at ETSIT-UPM, Spain, and his PhD degree at Universidad Rey Juan Carlos, Spain. He is currently Associate Professor at the Department of Signal Theory and Communications of Universidad de Alcalá de Henares, Spain, where he is involved in several undergraduate and master courses in Telecommunications Engineering. He has been Visiting Researcher at the Politectnico di Torino, Italy, and at the EPFL, Switzerland. His research activities are focused on Communications Systems and Information Theory, mainly on the topics of channel coding, modulation and multiple access, and on the applications of Chaos in Engineering.

Georges Kaddoum (M'11) received the Bachelor's degree in electrical engineering from the École Nationale Supérieure de Techniques Avancées (ENSTA Bretagne), Brest, France, and the M.S. degree in telecommunications and signal processing (circuits, systems, and signal processing) from the Université de Bretagne Occidentale and Telecom Bretagne(ENSTB), Brest, in 2005 and the Ph.D. degree (with honors) in signal processing and telecommunications from the National Institute of Applied Sciences (INSA), University of Toulouse, Toulouse, France, in 2009. Since november 2013, he is an Assistant Professor of electrical engineering with the École de Technologie Supérieure (ETS), University of Quebec, Montréal, QC, Canada. In 2014, he was awarded the ETS Research Chair in physical-layer security for wireless networks. Since 2010, he has been a Scientific Consultant in the field of space and wireless telecommunications for several companies (Intelcan Techno-Systems, MDA Corporation, and Radio-IP companies). He has published over 80 journal and conference papers and has two pending patents. His recent research activities cover wireless communication systems, chaotic modulations, secure transmissions, and space communications and navigation. Dr. Kaddoum received the Best Paper Award at the 2014 IEEE International Conference on Wireless and Mobile Computing, Networking, and Communications, with three coauthors, and the 2015 IEEE Transactions on Communications Top Reviewer Award.

Alexandre Wagemakers received the Telecommunication Engineering degree in 2003 from the Polytechnic University in Madrid, Spain, and the Ph.D. degree in Applied Physics in 2008 from the University Rey Juan Carlos, Madrid, Spain, where he is working as an Assistant Professor in the Department of Physics. His interest are currently the theory and applications of Nonlinear Dynamics.

Pascal Giard received the B.Eng. and M.Eng. degree in electrical engineering from École de technologie supérieure (ÉTS), Montreal, QC, Canada, in 2006 and 2009. From 2009 to 2010, he worked as a research professional in the NSERC-Ultra Electronics Chair on 'Wireless Emergency and Tactical Communication' at ÉTS. He is currently working toward the Ph.D. degree at McGill University. His research interests are in the design and implementation of signal processing systems with a focus on modern error-correcting codes.